Mechanical Systems and Signal Processing 108 (2018) 304–316

Contents lists available at ScienceDirect

Mechanical Systems and Signal Processing

journal homepage: www.elsevier.com/locate/ymssp

Analysis and experiment of magneto-mechanically coupled harvesters

P.V. Malaji [a,*], Shaikh Faruque Ali [b]

[a] Department of Mechanical Engineering, BLDEA's V.P Dr. P.G.H CET, Vijayapur 586101, India
[b] Department of Applied Mechanics, IIT Madras, Chennai 600036, India

ARTICLE INFO

Article history:
Received 1 August 2017
Received in revised form 4 February 2018
Accepted 13 February 2018

Keywords:
Pendulums
Electromagnetic energy harvesting
Broadband energy
Magneto-mechanical coupling

ABSTRACT

Current trend in energy harvesting research is to increase the operating bandwidth of energy harvesters. Multiple harvesters, nonlinear harvesters and hybrid harvesters are suggested to address the issue. In this paper, a system consisting of two electromagnetic harvesters with magnetic and mechanical couplings subjected to harmonic support excitations is proposed. Two pendulums with close resonating frequencies are used to generate power over a broad range of frequencies. The pendulums behave nonlinearly under the influence of magnetic interaction. This nonlinear motion harvests power at broader bandwidth. A mathematical model of the proposed harvester is established. Experiments are performed to validate the theoretical results. It has been observed that the nonlinear responses due to both magnet and mechanical couplings improve individual harvester performance. This is advantageous over harvesters that have magnetically coupling only. Additionally, the dynamics of harvesting system is numerically studied where large amplitude chaotic motion, quasi-periodic oscillations and periodic motions are observed and reported.

1. Introduction

Recent developments in automation, wireless technology and smart systems have necessitated the development of self- and low-powered sensors. Energy harvesting based batteryless devices have become more attractive and serve as an alternative to battery powered devices. Energy harvesting involves scavenging ambient energy and transforming them into electrical energy, either for immediate use by the sensors or stored in capacitors for later usage [1,2]. Conventional linear harvesters are efficient only at resonance, which limits their applications for almost all practical vibration sources with broadband or uncertain frequency content [3,4].

To overcome the bandwidth constraint of the linear harvesters, designs with tuning mechanisms to deal with uncertainty in natural frequencies and broadband spectra are studied. Various tuning methods have been proposed (for example, passive [5] and active [6]) to adaptively tune to the source frequency. Tuning is useful when the host frequency is unknown and is within a narrow band of the frequency. The disadvantage of tuning mechanisms is that most of them require an external power sources which reduces the net power obtained from the harvester [6].

Extensive studies exploring nonlinear structural designs to harvest broadband power are also reported [7–9]. Nonlinearity induced by magnetic interaction to provide monostable, bistable and tristable configurations has also been reported. A

* Corresponding author.
E-mail address: pradeepmalaji@bldeacet.ac.in (P.V. Malaji).

https://doi.org/10.1016/j.ymssp.2018.02.025
0888-3270/

Moon's beam under magnetic field has shown potential for broadband harvesting [7,8,10]. Enhancement in bandwidth is achieved by matching trajectories of cantilever tip magnets with that of the side magnets [11]. Internal resonance of a beam is also explored for broadband harvesting [12,13]. A periodic time-varying damping can also enhance bandwidth [14]. Structural instability due to buckling has been analyzed for broadband harvesting [9].

Another way to increase bandwidth is to use multiple or multi-modal harvesters [15]. Multimodal harvesters can harvest power at multiple modes effectively either with an additional mass on the harvester [16] or with a folded geometry of the harvesters [17]. While a close eigenmode provides a broadband application with lower power output, a large frequency gap between the modes makes these harvesters ineffective for harvesting power over a continuous frequency band [18]. Mechanical coupling of these multiple harvesters enhances both the magnitude and bandwidth of power [19]. Multiple harvesters with magnetic coupling between them also have been reported for broadband harvesting [20,21]. Effect of both magnetic and mechanical coupling together on the power magnitude and bandwidth needs to be explored.

Inspired by recent advances in harvesting with multiple coupled harvesters, this article reports a magneto-mechanically coupled harvesters to increase the bandwidth. The harvesting system consists of two pendulums with magnets attached at the free end for electromagnetic harvesting. The magnetic force on the oscillators due to magnets at the base is calculated based on point magnets and dipole approximation. The method provides considerably accurate results when the physical dimensions of magnets are small compared to the distance between them [22,23]. The magnetic force on the oscillator due to magnets at the base can also be obtained experimentally and via curve fitting [24,25]. Though this method evaluates the magnetic interaction well enough, conducting experiments is time consuming especially when the distance between the magnets needs to be changed frequently.

In this work, pendulums are chosen such that they have close natural frequencies in the magnetic field. The dynamics of the system due to magneto-mechanical coupling is reported and advantages in energy harvesting are drawn. It has been observed that the system of two pendulums shows interesting dynamics ranging from large orbit chaotic oscillation to quasi periodic motion and to low amplitude periodic motions under harmonic support excitation. Experiments are conducted to access the amount of power drawn and its frequency.

The flow of the paper is as follows. A mathematical model for a two pendulum harvesting system with magnetic and mechanical coupling is developed in Section 2. Section 3 presents the numerical study of the harvesting system. A discussion on the numerical study is presented in Section 4. Section 5 presents experimental results to support the numerical study. Based on the study a set of conclusions are drawn in Section 6.

2. Magneto-mechanical model of the harvester

This section reports the mathematical model of the harvesting system with magnetic interactions between mechanically coupled pendulums. As shown in Fig. 1, the mechanical coupling is obtained using spring arrangement between the pendulums and between the support and pendulum. The pendulums are coupled and grounded by mechanical springs k_1, k_2 and k_3. The spring between the pendulums is referred to as a coupling spring and the springs between the support and each pendulum is referred to as a grounding. The system is analyzed and tested under harmonic support excitation (x_g) given at the pivot.

Pendulums considered are of lengths l_1 and l_2. A permanent magnet is attached at the tip of each pendulum. The magnets are oriented such that they face the same polarity and are modeled as dipoles [23]. The repulsive force in the magnets depends upon the relative position between magnetic dipoles (r). Copper coils are placed beside the pendulums to harvest electromagnetic energy.

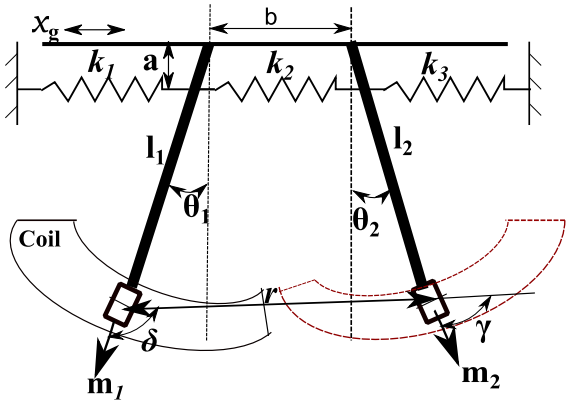

Fig. 1. Schematic representation of magneto-mechanically coupled harvester model.

As discussed in the previous section, the force due to magnetic interaction between the pendulums can be obtained either experimentally [24,25], or analytically [22,23]. In this article, magnets are assumed to be dipoles. The dipole model provides better values only when the distance between magnets is more than the dimension of magnets ([22]). In this article, the distance between magnets is kept sufficiently large than that of the larger dimension of the magnets.

The dimensions of the magnets are smaller than the length of pendulums and hence the magnet mass and the length are considered as a part of the pendulum mass and length respectively. Neglecting the frictional effect at the pivot, the equations of motion for the two pendulum harvesting system are given as follows [23];

$$\begin{aligned} I_1\ddot{\theta_1} + (c_m + c_e)l_1^2\dot{\theta_1} + m_1 g\frac{l_1}{2}\sin\theta_1 + k_1a^2(\sin\theta_1)\cos\theta_1 + k_2a^2(\sin\theta_1 - \sin\theta_2)\cos\theta_1 + M_{m1} = -m_1l_1\ddot{x_g}\cos\theta_1 \\ I_2\ddot{\theta_2} + (c_m + c_e)l_2^2\dot{\theta_2} + m_2 g\frac{l_2}{2}\sin\theta_2 + k_3a^2(\sin\theta_2)\cos\theta_2 + k_2a^2(\sin\theta_2 - \sin\theta_1)\cos\theta_2 + M_{m2} = -m_2l_2\ddot{x_g}\cos\theta_2 \end{aligned} \quad (1)$$

where, M_{m1}, M_{m2} are the derivatives of magnetic potential with respect to angular displacements θ_1 and θ_2 respectively. Expressions of M_{m1} and M_{m2} are given in the Appendix. Maple® is used to derive the expression for the magnetic moments. c_m and c_e are the mechanical and electrical damping respectively. The rotational moments of inertia of the pendulums are given as I_1 and I_2. Acceleration input to the pivot is $\ddot{x}_g$.

Fig. 2 shows the stable equilibrium positions of the pendulums with magnetic interaction. As the magnets are in the repulsive mode, the stable equilibrium positions are away from the vertical zero position. At lower values of pivot distance, b the pendulums remain away but with an increase in pivot distance, $\theta_1 = \theta_2 = 0$ turns to be the stable equilibrium position. For a symmetric system, $k_1 = k_3$ and $l_1 = l_2$, the stable equilibrium positions of pendulums are symmetric about zero. Asymmetry in the system can be introduced by changing the stiffness of the ground springs or the length of any one of the the pendulum. This asymmetry changes the natural frequencies of the pendulums, which results in enhancing the frequency band of the harvesting system. The parameters used for numerical simulations and experimental studies are given in Table 1.

Voltage induced due to electromagnetic induction is given as

$$v_i = \xi B_s L l_i \dot{\theta}_i \qquad i = 1, 2. \quad (2)$$

where L is the effective coil length, ξ is the filling factor of the coil. A filling factor or fill factor is the ratio of an actual volume of insulation wire used for winding to the volume of the coil used [26]. A dense winding provides better efficiency. B_s is the surface magnetic flux density. The average power harvested across the load resistance R_L is given as;

$$P_{i(avg)} = \frac{v_i^2}{R_L} \quad (3)$$

3. Numerical study on various harvester configurations

Numerical simulations are carried out on the analytical formulation to understand the effect of various parameters on the harvested energy and its bandwidth. Nonlinear equations of motion (given in Eq. (1)) of the harvesting system are solved numerically in MATLAB®. The nonlinear differential equations are represented as;

$$\dot{X} = f(X, t) \quad (4)$$

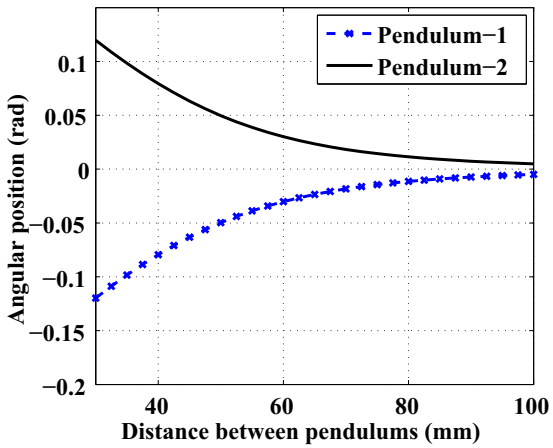

Fig. 2. Equilibrium positions of two identical pendulums with magnetic interaction.

Table 1
Parameters for numerical and experimental studies.

$c_1; c_2$	Mechanical damping coefficients of pendulums	0.004 Ns/m
$c_{e1}; c_{e1}$	Electrical damping coefficients	0.002 Ns/m
$l_1; l_2$	Length of pendulums (including magnet)	60 mm
$m_1; m_2$	Mass of pendulums (including magnet)	13 gm
a	Distance between the spring and hinge	20 mm
B_r	Residual magnetic flux	0.6 T
R_c	Coil resistance	160 Ω
ξ	Coil filling factor	0.3
–	Number of coil turns	3600
–	Magnet size (diameter and thickness)	10 mm × 10 mm

where X is the state vector, given as $X = \{\theta_1, \dot{\theta}_1, \theta_2, \dot{\theta}_2\}^T$. Detailed expression of $f(X,t)$ is given in the Appendix.

To access the benefits and advantages of magneto-mechanical coupling of pendulum harvesters, various configurations are numerically and experimentally tested. These are (i) independent harvesters (*i.e.* without magnetic interaction and mechanical coupling, $k_2 = 0$) (IH), (ii) magnetically coupled harvesters without mechanical coupling, $k_2 = 0$ (MCH), (iii) mechanically coupled harvesters (*i.e.* without magnetic interaction) (mCH) and (iv) magneto-mechanically coupled harvester (MmCH).

Fig. 3 shows power outputs from tuned pendulums at an excitation magnitude of 2.3 mm. Figs. 3(a) and (b) are same as the pendulums behave independently in absence of the coupling spring. For a smaller distance between the pendulum pivots ($b = 55$ mm) the harvesters exhibit nonlinear behavior characterized by a wider bandwidth and lower power output. At a larger distance between the pivots ($b = 100$ mm) the power output is characterized by a dominant single peak and a high power output, like a linear harvester. This is because of no or negligible magnetic interaction at larger pivot distance. The non-smoothness in the power curves may be due to the presence of quasi-periodicity. Figs. 3(a) and (b) show that both the pendulums harvester power at same frequency range and hence may not be useful for a broadband harvesting. Next section reports the effect of parameters on the harvested power and frequency bandwidth of the harvester.

3.1. Parametric study of the harvesting system

The objectives of this manuscript are to observe the effect of parameters on the amount of power harvested by the harvesting system and to broaden the frequency range over which power is harvested. Natural frequencies of the system form an important parameter to observe. As reported in [19,23], a tuned system that has same natural frequencies for the pendulums would have a narrower bandwidth. Similarly, if the natural frequencies of the pendulum are far apart from each other then power is harvested at two distinct frequencies which also do not serve as broadband energy harvesting. It is important to characterize the harvester based on its natural frequencies. Natural frequencies of the pendulums are varied by changing the stiffness of one ground spring (either k_1 or k_3). This method of changing natural frequencies is preferred over the change in length to maintain the same magnetic interaction. Stiffness of the ground spring connected to the second pendulum (k_3) is kept constant and stiffness of the ground spring connected to the first pendulum (k_1) is varied in this article. The ratio $\frac{k_1}{k_3}$ is considered between 1 and 3 that produced a linearly (approximately) varying frequency ratio $\frac{\omega_1}{\omega_2}$ between 1 and 1.28. Four

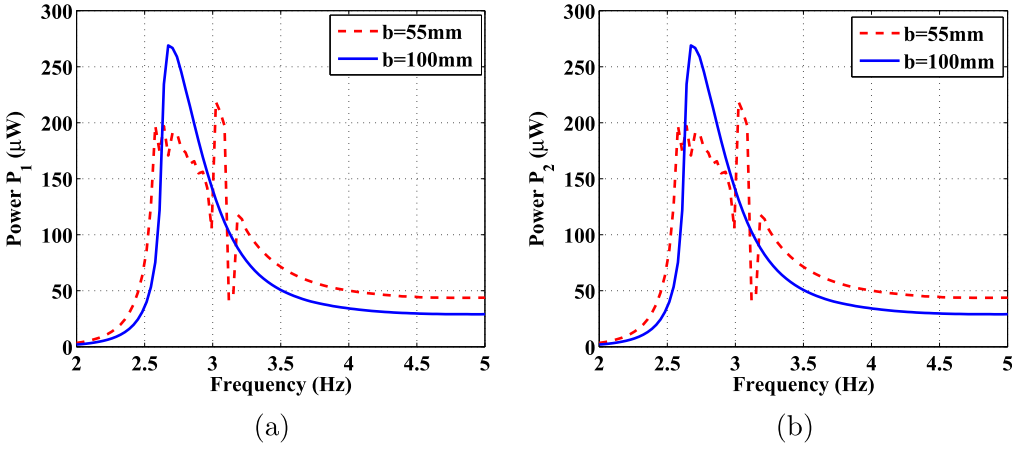

Fig. 3. Power curves for two pendulum harvester at $x_g = 2.3$ mm, $b = 55$ mm, $k_1 = k_3 = 4$ N/m and $k_2 = 0$. (a) Pendulum–1 and (b) Pendulum–2.

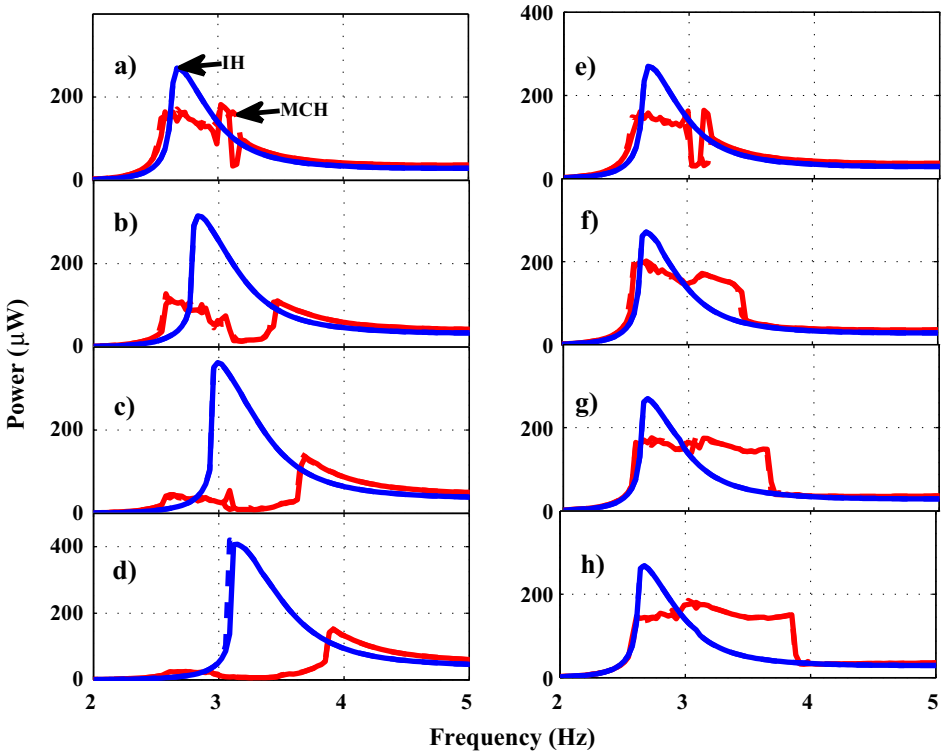

Fig. 4. Power harvested with $k_2 = 0, x_g = 2.3$ mm at various frequency ratios; (a–d) show power from Pendulum–1, (e–h) show power from Pendulum–2. (a & e) for $\omega_1/\omega_2 = 1$; (b & f) for $\omega_1/\omega_2 = 1.071$; (c & g) for $\omega_1/\omega_2 = 1.13$; (d & h) for $\omega_1/\omega_2 = 1.2$. (Solid line - forward sweep, dotted line - reverse sweep. Blue lines - IH ($b = 100$ mm), Red lines - MCH ($b = 55$ mm). (For interpretation of the references to colour in this figure legend, the reader is referred to the web version of this article.)

values of frequency ratio ($\frac{\omega_1}{\omega_2}$) are considered for observation. All numerical studies are carried out with harmonic excitation at the pivot with forward and reverse frequency sweeps. The amplitude of excitation is kept constant at 2.3 mm.

3.1.1. Results of Independent harvesters (IH) and magnetically coupled harvesters (MCH)

A comparison of power harvested over a frequency range under harmonic excitation is shown in Fig. 4 for four different spring constants, k_1 which provided four different sets of natural frequencies for the system. Since k_1 is varied keeping k_3 constant, the eigen-frequency related to pendulum–1 has changed but eigen-frequency of pendulum–2 remained constant.

As expected, Figs. 4(a)–(d), which are for pendulum–1 show a shift in the frequency at which peak power is obtained. The figures also show an increase in power magnitude for pendulum–1 with an increase in natural frequency. The power magnitudes for pendulum–2 shown in Figs. 4(e)–(h) remain unchanged.

Introduction of magnetic coupling changes the harvester characteristic (shown with a red colored curves in Fig. 4). A significant improvement in the bandwidth at $\frac{\omega_1}{\omega_2} = 1.2$ (an increase of 130% between 0.5 Hz to 1.26 Hz at 80 μW compared to IH) of pendulum–2 with a small reduction in power magnitude is observed. In case of pendulum–1, both power magnitude and bandwidth decreases (a 300% reduction in power and a 40% reduction in bandwidth at 80 μW compared to IH).

The improvement in pendulum–2 performance can be attributed to magnetic coupling between the pendulums. When the frequency is swept between two near resonances of the pendulums, the energy from pendulum–1 with slightly higher resonance frequency ($\frac{\omega_1}{\omega_2} = 1.2$) is transferred to pendulum–2. In this case, pendulum–1 can be used just as a magnetic oscillator and power can be harvested only from pendulum–2 as discussed by Tang and Wang [27]. It can also be noted that certain trade-off can be arrived at such that bandwidth increase in pendulum–2 negates the decrease in bandwidth and power in pendulum–1 by properly selecting the parameters.

Magnetic coupling of the harvesters has resulted in bandwidth improvement in the pendulum with lower natural frequency and lost efficiency in the pendulum with higher natural frequency. Next subsection reports on the effect of mechanical coupling on harvester performance in the absence (mCH) and presence (MmCH) of magnetic coupling.

3.1.2. Results on mechanically coupled (mCH) and magneto-mechanically coupled (MmCH) harvesters

Figs. 5(a)–(h) show the power plots obtained for mechanically coupled pendulums and magneto-mechanically coupled pendulums under harmonic support excitation for various frequency values. Results with $\frac{\omega_1}{\omega_2} = 1.071$ is reported in the study.

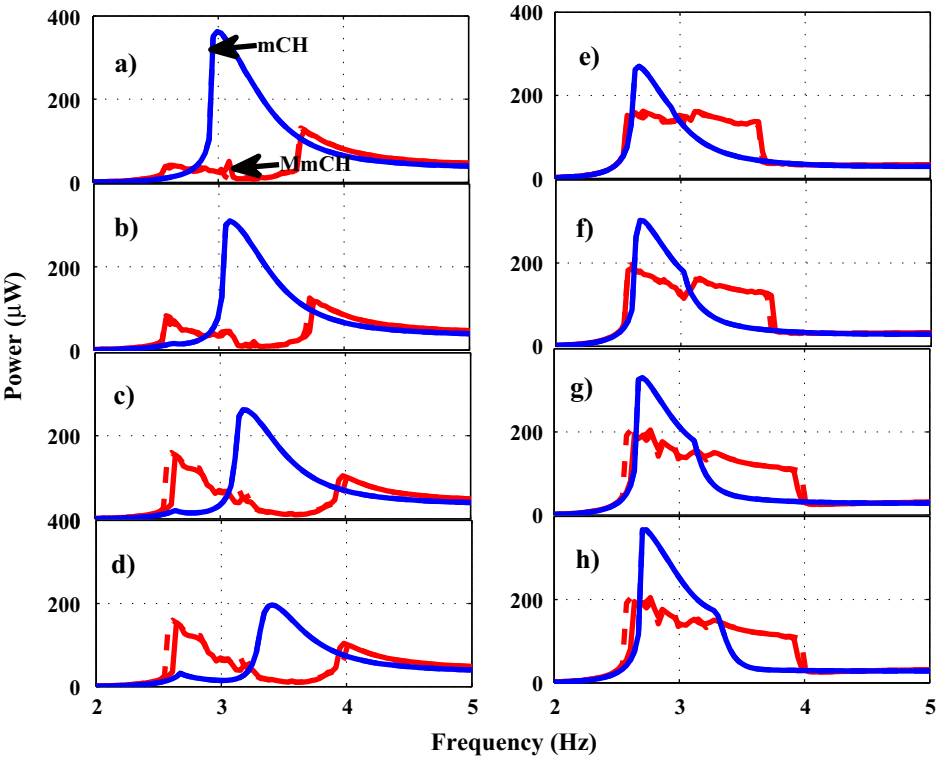

Fig. 5. Power harvested at $x_g = 2.3$ mm and $b = 55$ mm for $\omega_1/\omega_2 = 1.071$ at various coupling spring stiffness. (a–d) power from pendulum–1, (e–h) power from pendulum–2. (a & e) $k_2 = 0$, (b & f) $k_2 = 0.5$, (c & g) $k_2 = 1$, (d & h) $k_2 = 2$. (Solid line - forward sweep, dotted line - reverse sweep. Blue lines - mechanical coupling, Red lines - magneto mechanical coupling. (For interpretation of the references to colour in this figure legend, the reader is referred to the web version of this article.)

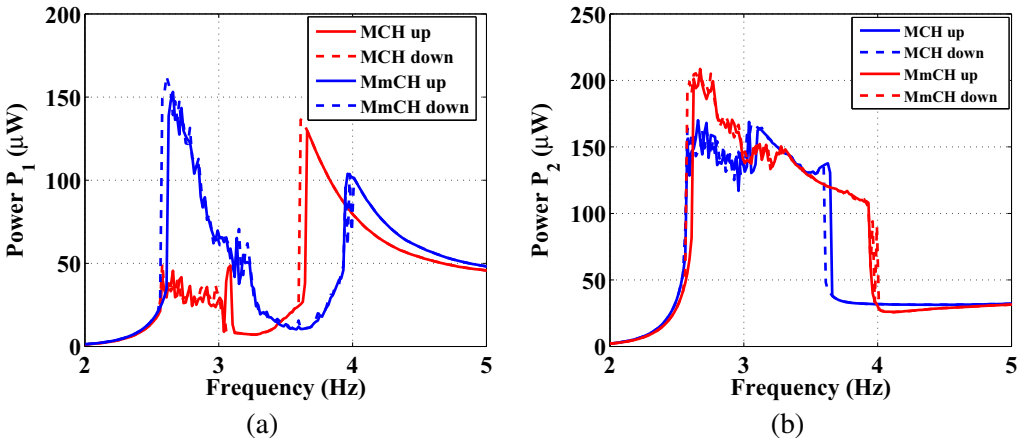

Fig. 6. Comparison of power harvested from MCH and MmCH harvesting systems, for $\frac{\omega_1}{\omega_2} = 1.071$ and $b = 55$ mm (a) power curves obtained in pendulum–1 (b) power curves obtained in pendulum–2. (up - forward, down - reverse sweep).

It is to be noted that mechanical coupling is arrived at using a spring of stiffness k_2 between the pendulums. For an independent set of harvesters ($k_2 = 0$) pendulum–1 with higher natural frequency harvests more power compared to pendulum–2 as shown in Figs. 5(a) and (e) (blue colored lines). With an introduction of the mechanical coupling ($k_2 \neq 0$), the harvesting system converts to a coupled two degree of freedom system with two natural frequencies. Therefore resonating frequencies of both the pendulums change. This can be observed in Fig. 5 (with blue colored lines).

Introduction of the mechanical coupling in presence of magnetic coupling (MmCH) enhances the bandwidth of both the pendulums (shown with red lines in Fig. 5). MmCH enhances performances of both the harvesters compared to mCH. This improvement in pendulum–1 performance can be attributed to the bi-modal response due to mechanical coupling in the

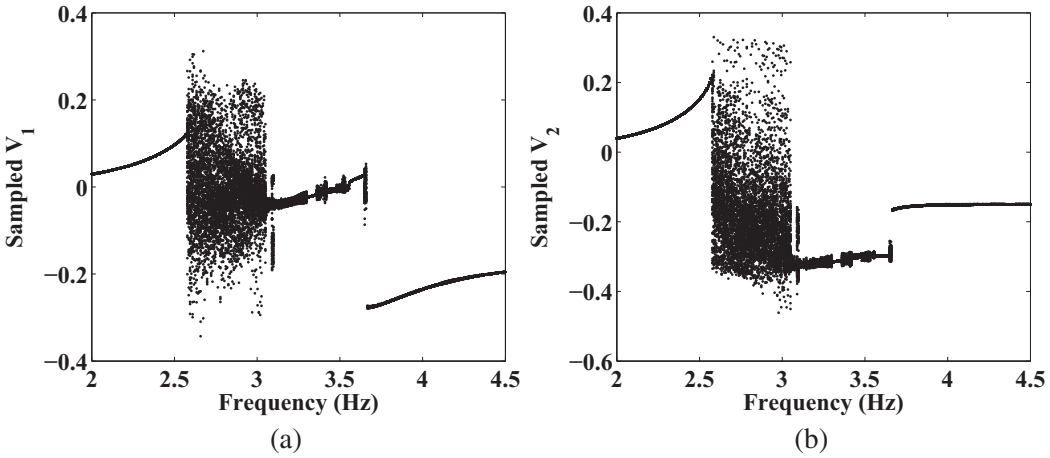

Fig. 7. Bifurcation diagrams of voltage output *w.r.t.* frequency without mechanical coupling $k_2 = 0, \frac{\omega_1}{\omega_2} = 1.071, b = 55$ mm; (a) voltage in Pendulum–1 (b) voltage in Pendulum–2.

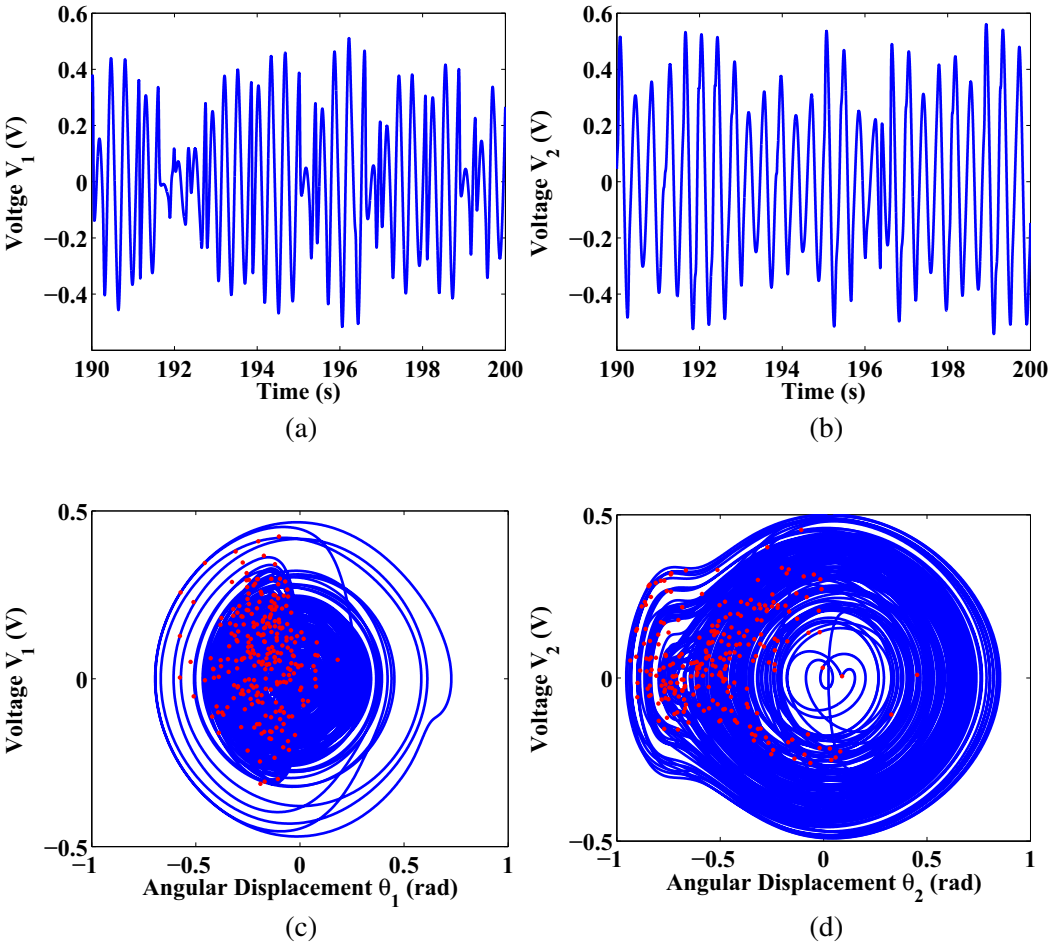

Fig. 8. Voltage time histories and phase portraits at 2.6 Hz excitation frequency. (a & c) responses for Pendulum–1 (b & d) responses for Pendulum–2. The phase portraits show poincare dots representing chaotic motion.

presence of magnetic interaction. The magnitude and frequency band at first mode due to mechanical coupling is enhanced by magnetic coupling.

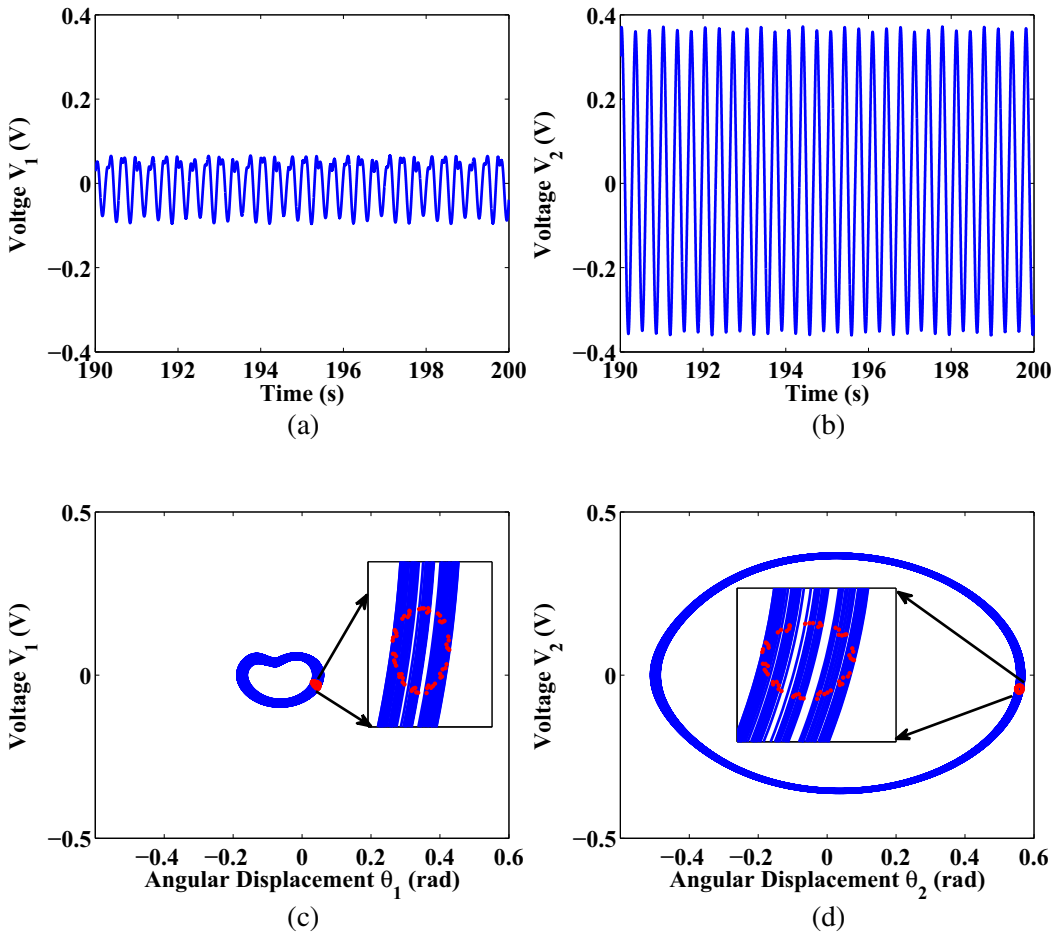

Fig. 9. Voltage time histories and phase portraits at 2.96 Hz excitation frequency. (a & c) responses for Pendulum–1 (b & d) responses for Pendulum–2. The phase portraits show circular poincare dots representing quasi periodic motion. Note the low amplitude motion in pendulum–1.

3.1.3. Results on magnetically coupled (MCH) and magneto-mechanically coupled (MmCH) harvesters

A comparison of power harvested with a magnetic coupling (MCH) and with a magneto-mechanical coupling (MmCH) is shown in Fig. 6. Enhancements in both power magnitude and bandwidth are observed when a mechanical coupling is present along with magnetic coupling. Increments of 40% (0.5 Hz to 0.69 Hz) and 28% (1.12 Hz to 1.4 Hz) in bandwidth at 80 μw is observed for pendulum–1 and pendulum–2 respectively for MmCH compared to MCH. Peak power in pendulum–1 is increased by 100% and pendulum–2 by 50% compared to MCH.

The bandwidth of the pendulum–1 for MmCH remains almost the same but the peak power decreased from 415 μW in IH to 166 μW. Power bandwidth in pendulum–2 for MmCH increased by 180% (from 0.5 Hz in IH to 1.4 Hz) with a slight decrease in peak power (from 236 μW in IH to 216 μW). Hence both mechanical and magnetic coupling enhanced the power harvesting capabilities of the harvester.

4. Discussion on the numerical studies MCH and MmCH

The previous section detailed the power obtained and broadband nature of every configuration that are possible in the two pendulum harvesting system. Possible advantages and disadvantages are drawn. The estimated power is an average power of the simulation that has been run until the steady state is reached. The simulations are run for 200s and RMS voltage of entire 200s are considered for the analysis. It has been observed that increasing the time duration for calculating average power has not reduced the non-smoothness nature of the power curves neither it has any effect on the broadband nature of the curves. This section focuses on the dynamics of the two pendulum energy harvesting system.

Fig. 7 shows the voltage dynamics of both the pendulums. The excitation frequency ranging from 0.1 to 5 Hz is considered with a step size of 0.005 Hz. Fig. 7 shows responses of nonlinear oscillations of the mechanically uncoupled pendulums with $k_2 = 0, \frac{\omega_1}{\omega_2} = 1.071$ and $x_g = 2.3$ mm. Bifurcation in the voltage diagram is clear. It can also be observed from Fig. 7 that the

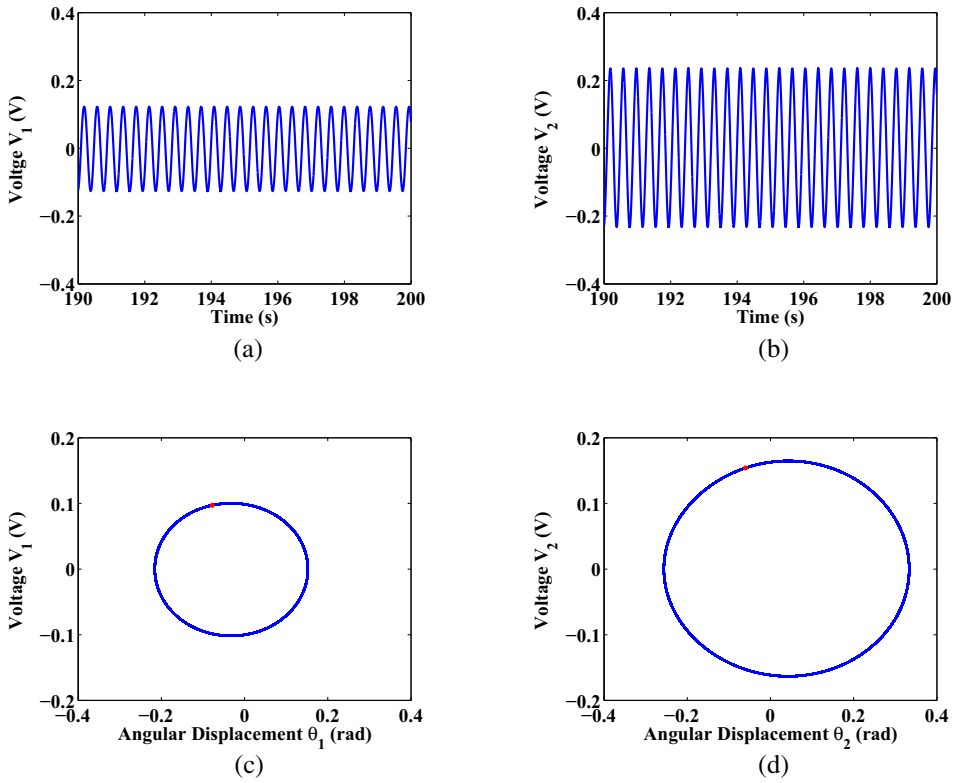

Fig. 10. Voltage time histories and phase portraits at 3.1 Hz excitation frequency. (a & c) responses for Pendulum–1 (b & d) responses for Pendulum–2. The phase portraits show low amplitude periodic motion.

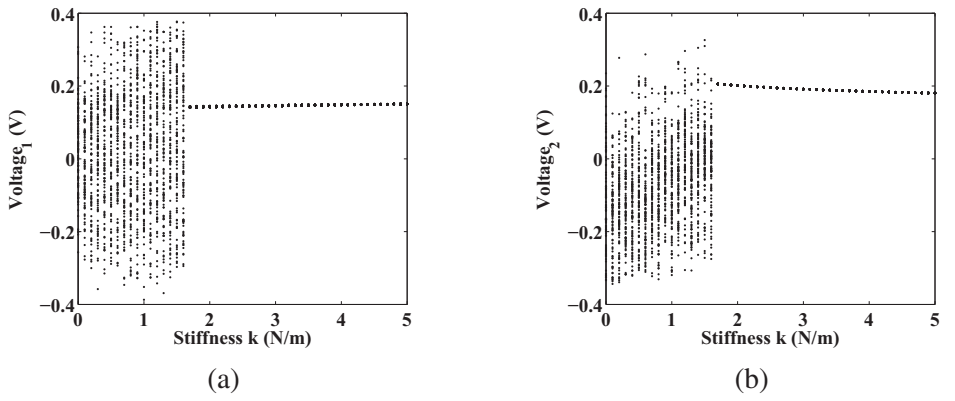

Fig. 11. Bifurcation diagrams of voltage plotted against mechanical coupling at $\omega = 2.6$ Hz, $b = 55$ mm and $\frac{\omega_1}{\omega_2} = 1.071$. (a) response for Pendulum–1 (b) response for Pendulum–2.

pendulums enter into the high-energy orbit through chaos and keep large-amplitude motion over a bandwidth of 2.58–3.1 Hz generating high voltages. Pendulum–1 again enters periodic large amplitude motion for a shorter frequency range around 3.63 Hz. Whereas pendulum–2 continues under slightly large amplitude motion up to 3.67 Hz indicating enhanced bandwidth.

Voltage time history plots and phase portraits at 2.6 Hz excitation frequency are shown in Fig. 8. At this excitation frequency, the system exhibits large amplitude chaotic response. This is evident from Figs. 8(c) and (d) that show phase portraits of the voltage against angular displacement for both the pendulums. The Poincare dots (in red color) show that the system is undergoing large amplitude chaotic motion. After the large amplitude chaotic motion the pendulums enter into small amplitude periodic oscillations through quasi-periodic motion as shown in Fig. 9 which is the response of the system at 2.96 Hz excitation frequency. The closed orbit Poincare dots on phase portraits shown in Figs. 9(c) and (d) indicate the

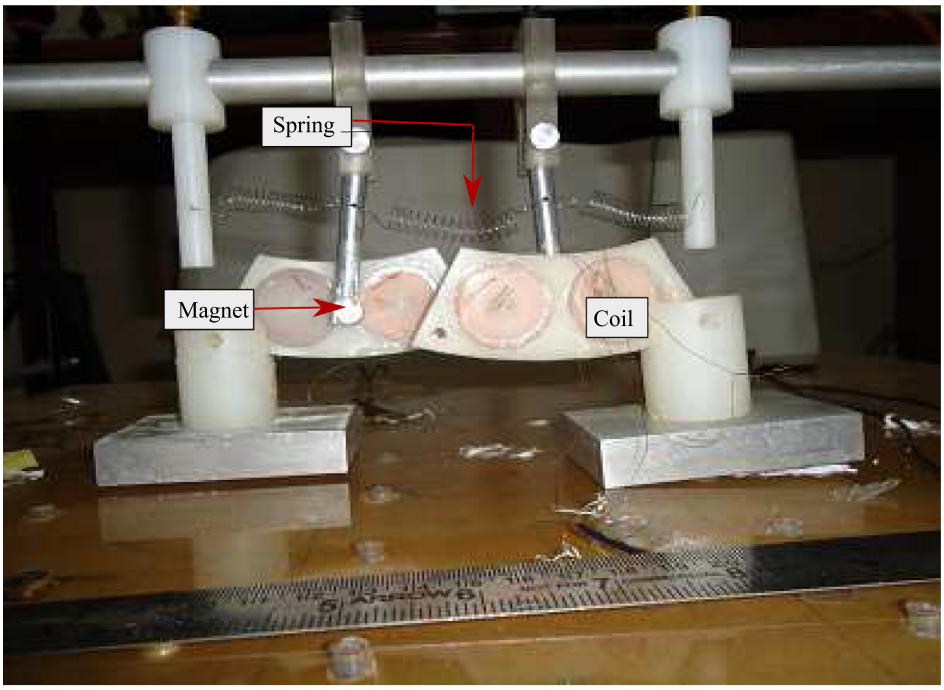

(a)

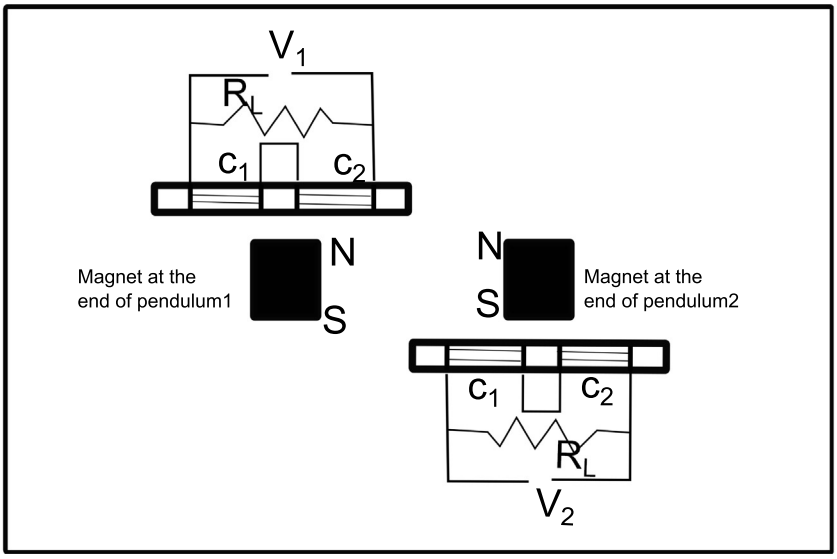

(b)

Fig. 12. Details of the experimental set-up. (a) Two pendulum harvester and the coils set; (b) schematic plan of coil set and magnet arrangement.

presence of quasi-periodic motion. Figs. 9(a) and (b) show the voltage time history of the pendulums. Pendulum–1 shows small amplitude motion at 2.96 Hz excitation frequency whereas Pendulum–2 still shows large amplitude motion.

Fig. 10 shows voltage time histories and phase portraits of the pendulums at 3.1 Hz excitation frequency. The system exhibits periodic response with a very low voltage output. A transition from high voltage chaos showing a torus losing its form giving rise to a low voltage periodic response indicates quasi periodic route.

Fig. 11 shows the bifurcation diagrams of the voltages in pendulum–1 and pendulum–2 for different values of coupling spring stiffness at an excitation frequency $\omega = 2.6$ Hz. Due to magnetic interaction high magnitude chaotic response is

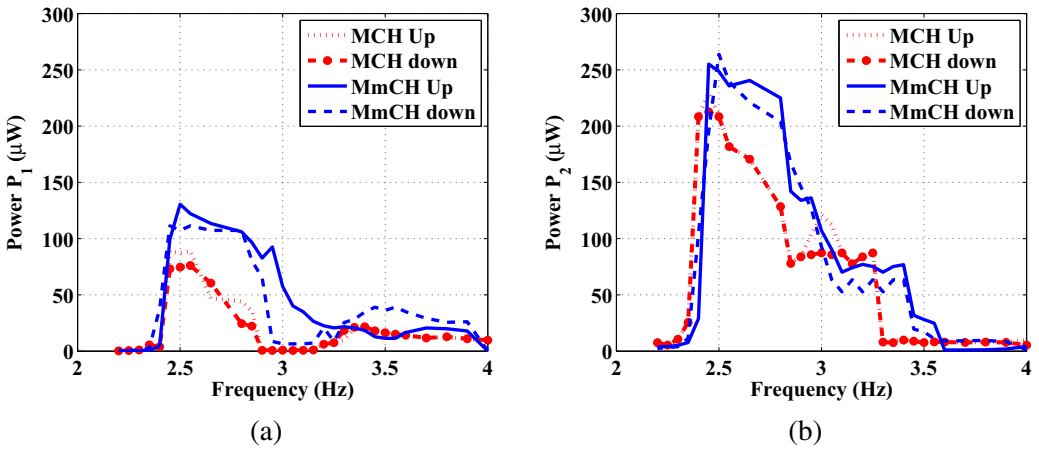

Fig. 13. Experimental response curves with magnetic coupling (MCH) and magneto-mechanical coupling (MmCH). Bandwidth observed at 70 μW, for Pendulum–1 is MCH: 2.45–2.65 Hz & MmCH: 2.5–3 Hz; and for Pendulum–2 is MCH: 2.35–3.25 Hz & MmCH 2.35–3.45 Hz. Up represents forward sweep and down represents backward sweep.

observed in voltage for a coupling stiffness up to 1.8 N/m. For stronger coupling stiffness the voltage magnitude decreases and a periodic response is observed. Stronger mechanical coupling eliminates the relative motion between pendulums hence reducing the high amplitude chaotic response due to magnetic interaction. Next section describes the experiments carried out on the two pendulum harvesting system.

5. Experimental results and discussion

This section describes the experiments conducted with magneto-mechanically coupled harvesters (MmCH). Fig. 12(a) shows a close-up view of the harvester with two pendulums. Pendulums are pivoted to the shaft at a preset distance. Springs are connected. Since the pendulums move in a circular path, each pendulum is provided with a set having two coils (c_1 and c_2) to harvest electromagnetic energy. Since the coil set is longer in length, in order to avoid overlap of coils they have been placed at different sides of pendulums as shown in Fig. 12(a). More details on the experimental setup are available in [23]. Details of parameters used for the tests are given in Table 1.

Fig. 13 shows response curves for MCH and MmCH harvesting system. Forward and reverse frequency sweeps are conducted at a constant base excitation amplitude of 2.3 mm with different frequencies. The nonlinearity is quite evident from the responses, as there is no single resonance peak in the power curves. Pendulum–2 in MCH produces a power of 230 μW. The bandwidth in MCH is 0.9 Hz at a power magnitude of 70 μW. The bandwidth is calculated as the range of frequency at which the harvester can scavenge a constant power. Pendulum–1 produces lower power in MCH *ie* 91 μW. A bandwidth of 0.2 Hz at 70 μW is observed. Magnetic coupling alone broadens the operating bandwidth but magneto-mechanical coupling is observed to increase both bandwidth as well as the power harvested. The bandwidth of pendulum–1 at 70 μW is increased by 150% (0.2 Hz to 0.5 Hz) for MmCH compared to MCH only. Increase in power magnitude is from 91 μW to 136 μW. Bandwidth of pendulum–2 is also increased by 22% (0.9–1.1 Hz) at 70 μW, and the power scavenged is increased from 233 μW to 251 μW. The qualitative match between simulated (Fig. 6) and experimental (Fig. 13) results can also be observed. However, quantitative discrepancies exist.

6. Conclusion

This article presents a magneto-mechanically coupled pendulum harvester that can generate a high power output across a wider frequency bandwidth. A theoretical model is developed with point dipole approximations. Chaotic motion due to magnet interaction has been observed to enhance the vibration amplitude and power output when the excitation is between the two resonant frequencies. As frequency is increased a quasi periodic response is observed and then at even higher frequency a low amplitude periodic motion is seen. The horizontal distance between the magnets is also investigated and shown to have an influence on the bandwidth and power output from the harvester. The comparison between the simulation and experimental results shows qualitative agreement in the power output and bandwidth. This study demonstrates that the magneto-mechanically coupled energy harvesters with appropriate mechanical coupling can effectively improve the power output in a wider bandwidth for energy harvesting.

Acknowledgment

The authors are thankful to the Department of Science and Technology, India for funding the research work (Project No.: DST-YSS/2014/000336). The authors are also thankful to Prof. M. I. Friswell, Swansea University, UK for his valuable inputs.

Appendix A

The derivation of Eq. (1) needs calculation of magnetic force, which is presented here. Assuming the angle between the dipole axis and the line joining the dipole axis are δ and γ for Pendulum–1 and Pendulum–2 respectively (see Fig. 1 for details). δ and γ can be represented in terms of θ_1 and θ_2 as;

$$\cos(\delta) = \frac{b\sin(\theta_1) - l_1 b(1-\cos(-\theta_2+\theta_1))}{r}$$
$$\cos(\gamma) = \frac{b\sin(\theta_2) + l_2 b(1-\cos(-\theta_2+\theta_1))}{r}$$

Expression for $M_{m1} = M_{m2}$ i.e., derivative of magnetic potential with respect to θ_1 and θ_2 are given as,

$$M_{m1} = \frac{\mu_0(g_1 - g_2 + g_3 - g_4)}{4\pi r_n^3} - \frac{3\mu_0(g_5 - g_6)g_7}{8\pi r_n^5}$$

$$g_1 = -m^2\sin(-\theta_2+\theta_1)$$
$$g_2 = \frac{3}{r_n^2}m^2(b\cos(\theta_1) - l_1 b\sin(-\theta_2+\theta_1))(b\sin(\theta_2) + l_2 b(1-\cos(-\theta_2+\theta_1)))$$
$$g_3 = \frac{3}{r_n^4}m^2(b\sin(\theta_1) - l_1 b(1-\cos(-\theta_2+\theta_1)))(b\sin(\theta_2) + l_2 b(1-\cos(-\theta_2+\theta_1)))$$
$$(-2(b + l_2\sin(\theta_2) - l_1\sin(\theta_1))l_1\cos(\theta_1) + 2(l_2\cos(\theta_2) - l_1\cos(\theta_1))l_1\sin(\theta_1))$$
$$g_4 = \frac{3}{r_n^2}m^2(b\sin(\theta_1) - l_1 b(1-\cos(-\theta_2+\theta_1)))l_2 b\sin(-\theta_2+\theta_1)$$
$$g_5 = m^2\cos(-\theta_2+\theta_1)$$
$$g_6 = \frac{3}{r_n^2}m^2(b\sin(\theta_1) - l_1 b(1-\cos(-\theta_2+\theta_1)))(b\sin(\theta_2) + l_2 b(1-\cos(-\theta_2+\theta_1)))$$
$$g_7 = -2(b + l_2\sin(\theta_2) - l_1\sin(\theta_1))l_1\cos(\theta_1) + 2(l_2\cos(\theta_2) - l_1\cos(\theta_1))l_1\sin(\theta_1)$$

The complete expression of $f(X,t)$ in Eq. (4) is given below.

$$f(X,t) = \begin{bmatrix} x_2 \\ \frac{1}{I_1}\{-(c_m+c_e)l_1^2 x_2 - m_1 g\frac{l_1}{2}\sin x_1 - k_1 a^2(\sin x_1)\cos x_1 - \\ k_2 a^2(\sin x_1 - \sin x_3)\cos x_1 - M_{m1} - m_1 l_1 X_g\cos\omega t\cos x_1\} \\ x_4 \\ \frac{1}{I_2}\{-(c_m+c_e)l_2^2 x_4 - m_2 g\frac{l_2}{2}\sin x_3 - k_3 a^2(\sin x_3)\cos x_3 - \\ k_2 a^2(\sin x_3 - \sin x_1)\cos x_3 - M_{m2} - m_2 l_2 X_g\cos\omega t\cos x_3\} \end{bmatrix}$$

References

[1] C. Williams, R. Yates, Analysis of a micro-electric generator for microsystems, Proceedings of the International Solid-State Sensors and Actuators Conference – TRANSDUCERS '95 1 (1995) 8–11.
[2] J.A. Paradiso, T. Starner, Energy scavenging for mobile and wireless electronics, IEEE Pervasive Comput. 4 (2005) 18–27.
[3] S. Roundy, P.K. Wright, A piezoelectric vibration based generator for wireless electronics, Smart Mater. Struct. 13 (2004) 1131–1142.
[4] S.F. Ali, M.I. Friswell, S. Adhikari, Piezoelectric energy harvesting with parametric uncertainty, Smart Mater. Struct. 19 (2010) 1–9.
[5] V.R. Challa, M.G. Prasad, Y. Shi, F.T. Fisher, A vibration energy harvesting device with bidirectional resonance frequency tunability, Smart Mater. Struct. 17 (2008) 015035.
[6] S. Roundy, Y. Zhang, Toward self-tuning adaptive vibration based micro-generators, in: Proceedings of SPIE, vol. 5649, pp. 373–384.
[7] A. Erturk, J. Hoffmann, D.J. Inman, A piezomagnetoelastic structure for broadband vibration energy harvesting, Appl. Phys. Lett. 94 (2009) 1–4.
[8] S.F. Ali, S. Adhikari, M.I. Friswell, S. Narayanan, The analysis of piezomagnetoelastic energy harvesters under broadband random excitations, J. Appl. Phys. 109 (2011) 1–8.
[9] M.I. Friswell, S.F. Ali, O. Bilgen, S. Adhikari, A.W. Lees, G. Litak, Non-linear piezoelectric vibration energy harvesting from a vertical cantilever beam with tip mass, J. Intell. Mater. Syst. Struct. 23 (2012) 1505–1521.
[10] K.A. Kumar, S.F. Ali, A. Arockiarajan, Magneto-elastic oscillator: modeling and analysis with nonlinear magnetic interaction, J. Sound Vib. 393 (2017) 265–284.
[11] W. Deng, Y. Wang, Systematic parameter study of a nonlinear electromagnetic energy harvester with matched magnetic orientation: numerical simulation and experimental investigation, Mech. Syst. Signal Process. 85 (2017) 591–600.
[12] W. Yang, S. Towfighian, A hybrid nonlinear vibration energy harvester, Mech. Syst. Signal Process. 90 (2017) 317–333.

[13] H. Wang, F. Hu, K. Wang, Y. Liu, W. Zhao, Three-dimensional piezoelectric energy harvester with spring and magnetic coupling, Appl. Phys. Lett. 110 (2017) 1–5.
[14] M. Scapolan, M.G. Tehrani, E. Bonisoli, Energy harvesting using parametric resonant system due to time-varying damping, Mech. Syst. Signal Process. 79 (2016) 149–165, Special Issue from ICEDyn 2015.
[15] M. Rajarathinam, S. Ali, Energy generation in a hybrid harvester under harmonic excitation, Energy Convers. Manage. 155 (2018) 10–19.
[16] Q. Ou, X. Chen, S. Gutschmidt, A. Wood, N. Leigh, A.F. Arrieta, An experimentally validated double-mass piezoelectric cantilever model for broadband vibration–based energy harvesting, J. Intell. Mater. Syst. Struct. 23 (2012) 117–126.
[17] L.J. Gong, Q.S. Pan, W. Li, G.Y. Yan, Y.B. Liu, Z.H. Feng, Harvesting vibration energy using two modal vibrations of a folded piezoelectric device, Appl. Phys. Lett. 107 (2015) 1–5.
[18] I. Sari, T. Balkan, H. Kulah, An electromagnetic micro power generator for wideband environmental vibrations, Sens. Actuat. A 145–146 (2008) 405–413.
[19] P.V. Malaji, S.F. Ali, Broadband energy harvesting with mechanically coupled harvesters, Sens. Actuat. A: Phys. 255 (2017) 1–9.
[20] W.J. Su, W.Z. Jean, Design and development of a broadband magnet-induced dual-cantilever piezoelectric energy harvester, J. Intell. Mater. Syst. Struct. 0 (2013) 1–13.
[21] S. Zhou, J. Cao, W. Wang, S. Liu, J. Lin, Modeling and experimental verification of doubly nonlinear magnet-coupled piezoelectric energy harvesting from ambient vibration, Smart Mater. Struct. 24 (2015) 1–13.
[22] S.C. Stanton, C.C. McGehee, B.P. Mann, Nonlinear dynamics for broadband energy harvesting: Investigation of a bistable piezoelectric inertial generator, Physica D 239 (2010) 640–653.
[23] P.V. Malaji, S.F. Ali, Magneto-mechanically coupled electromagnetic harvesters for broadband energy harvesting, Appl. Phys. Lett. 111 (2017) 1–5.
[24] B. Mann, N. Sims, Energy harvesting from the nonlinear oscillations of magnetic levitation, J. Sound Vib. 319 (2009) 515–530.
[25] S. Zhou, J. Cao, A. Erturk, J. Lin, Enhanced broadband piezoelectric energy harvesting using rotatable magnets, Appl. Phys. Lett. 102 (2013) 1–4.
[26] A.J. Sneller, B.P. Mann, On the nonlinear electromagnetic coupling between a coil and an oscillating magnet, J. Phys. D: Appl. Phys. 43 (2010) 1–10.
[27] L. Tang, Y. Yang, A nonlinear piezoelectric energy harvester with magnetic oscillator, Appl. Phys. Lett. 101 (2012).